Combinatorially Prepared $[LiF]_{1-x}Fe_x$ Nanocomposites for Positive Electrode Materials in Li-Ion Batteries

Peng Liao,[†] Bretton L. MacDonald,[†] R. A. Dunlap,[†,‡] and J. R. Dahn*[,†,‡]

Department of Physics and Atmospheric Science, Dalhousie University, Halifax, N.S. B3H 3J5, Canada, and Institute for Research in Materials, Dalhousie University, Halifax, N.S. B3H 3J5, Canada

Received September 17, 2007. Revised Manuscript Received November 1, 2007

Nanocomposites of lithium fluoride and transition metals are promising new positive electrode materials for lithium-ion batteries. Libraries of $[LiF]_{1-x}[Fe]_x$ ($0 < x < 1$) nanocomposites were prepared by combinatorial cosputtering of lithium fluoride and iron. The sputtered libraries were characterized by X-ray diffraction (XRD) and ^{57}Fe Mössbauer effect spectroscopy to determine their micro- or nanostructure. At the Fe-rich end of the library ($x \approx 0.9$), a broad Fe (110) Bragg peak appears in the XRD patterns. Mössbauer spectra show that most of the Fe atoms are located within large Fe grains while a small number of Fe atoms are located in the interfacial region between Fe grains and small LiF regions. At the LiF-rich end of the library ($x \approx 0.1$), the LiF (111) peak was observed in the XRD pattern. Large LiF grains prevent the Fe atoms from aggregating, so the Fe grain sizes are so small that they exhibit paramagnetic properties in Mössbauer spectra. Some of the Fe atoms are also located in the interfacial region between small paramagnetic Fe grains and LiF grains. In the middle of the library ($x \approx 0.5$), XRD patterns do not show any Fe or LiF Bragg peaks, while Mössbauer spectra show that about half of the Fe atoms are aggregated into small grains, while the other half of Fe atoms are in the interfacial region. The electrochemical activities of the libraries were investigated using 64 electrode combinatorial electrochemical cells heated at 70 °C. The differential capacity versus potential curves show that lithium fluoride (very small x) and iron (very large x) do not show electrochemical activity, as expected, but that nanocomposites of lithium fluoride and iron exhibit significant electrochemical activities. When the LiF:Fe ratio is near 3, the second discharge capacity is about 620 mA h/g at 70 °C.

Introduction

Li-ion batteries are widely used in mobile electronic devices such as cell phones and laptop computers, and they are being targeted as a power source for electric vehicles. Currently lithium transition metal oxides are used for the positive electrode material in lithium-ion batteries.[1] The upper limit of the specific capacity of these materials is about 280 mA h/g. In order to satisfy the increasing energy demands for lithium-ion batteries, novel materials with larger specific capacity must be found. Recently, nanostructured materials utilizing displacement reactions have become the focus of study by a number of research groups.

The applicable displacement reaction for a nanoscale mixture of LiF and a transition metal, M, can be summarized as follows:

$$n\mathrm{LiF} + \mathrm{M} \leftrightarrow \mathrm{MF}_n + n\mathrm{Li}$$

During the charge process the metal is oxidized and metal fluorides are formed, while lithium ions and electrons are extracted from the positive electrode. During the discharge, the reaction is reversed so the active material is reduced to the metal and lithium fluoride is formed. Because all the oxidation states of the cation of the active material can be used in the reaction, displacement reactions can have specific capacities up to 700 mA h/g. Intimately mixed nanosized LiF and M grains are required for the displacement reactions to proceed reversibly.

An early work concerning displacement reactions for Li batteries appeared in 1969, where CuF_2 was proposed as a positive electrode material.[2] Recently, Maier's research group studied the lithium storage properties of some binary metal fluorides and oxides. Their work showed displacement reactions between lithium and binary metal fluorides or oxides could be quite reversible and could lead to a very high Li storage capacity.[3] Amatucci studied FeF_3:C nanocomposites, which exhibited a first discharge capacity of 660 mA h/g at 70 °C.[4]

Positive electrode materials for Li-ion batteries preferably contain all the needed lithium atoms for the cell reaction. Thus, it is preferable to prepare nLiF:M nanocomposites compared to MF_n, provided that the former can be demonstrated to perform well. Obrovac and Dahn studied the electrochemical activities of lithia/metal and lithium sulfide/metal nanocomposites and showed that reversible extraction of lithium could be performed.[5] Later, Amatucci showed that Li could be extracted from LiF:Bi:C nanocomposites and

* Corresponding author: Tel +1-902-494-2991; fax +1-902-494-5191; e-mail jeff.dahn@dal.ca.
† Department of Physics and Atmospheric Science.
‡ Institute for Research in Materials.

(1) Mizushima, K.; Jones, P. C.; Wiseman, P. J.; Goodenough, J. B. *Mater. Res. Bull.* **1980**, *15*, 783.
(2) Cairns, E. J.; Shimotake, H. *Science* **1969**, *164*, 1347.
(3) Li, H.; Balaya, P.; Maier, J. *J. Electrochem. Soc.* **2004**, *151*, A1878.
(4) Badway, F.; Cosandey, F.; Pereira, N.; Amatucci, G. G. *J. Electrochem. Soc.* **2003**, *150*, 1318.

10.1021/cm702656k CCC: $40.75
Published on Web 12/22/2007

subsequently reinserted.[6] In 2006, Fu's group reported electrochemical studies of LiF:Co and LiF:Ni nanocomposites prepared by pulsed laser deposition, but their LiF:Ni materials could only supply 107 mA h/g first charge capacity, much less than the expected 483 mA h/g for 2LiF:Ni (making NiF_2) nanocomposities.[7,8] Liao and Dahn studied the electrochemical activities of LiF:Ni nanocomposites by combinatorial sputtering and showed that this system could provide high specific capacities and good reversibility at room temperature.[9]

Currently while most of the research work is focused on the electrochemical activities of nanocomposites of lithium fluoride and transition metals, not much is known about the micro- or nanostructure of these materials. X-ray diffraction (XRD) is a powerful tool to characterize the microstructure of materials, but it may be insensitive to nanostructure of materials because nanometer-sized grains lead to extremely broad diffraction peaks. Mössbauer effect spectroscopy can provide detailed insight into the local structure surrounding Mössbauer active elements such as Fe and Sn and has the advantage of being able to probe the small-scale nanocrystalline structure that may appear to be amorphous by XRD. The combination of XRD and Mössbauer has become an important tool in the study of the structural properties of materials.[10,11] Recently, Bomio and co-workers identified Fe atoms within bulk particles and Fe atoms located at particle surface sites on the basis of Mössbauer analysis of reduced $NiFe_2O_4$ and $CuFe_2O_4$ electrodes. The percentage of interior Fe atoms at the end of second discharge was larger than that at the end of first discharge, suggesting that reduced Fe atoms tend to aggregate. This may be the cause of the loss of performance displayed by these electrodes.[12,13] Saeed and co-workers studied the influence of particle size, temperature, and measurement time scale on the transition from paramagnetic to ferromagnetic behavior of small particles of iron oxides.[14]

Combinatorial and high throughput materials science is now being adopted in the search for new materials, including better battery electrode materials.[15,16] Here, studies of $[LiF]_{1-x}Fe_x$ nanocomposites, prepared by combinatorial cosputtering of LiF and Fe targets in the presence of argon,

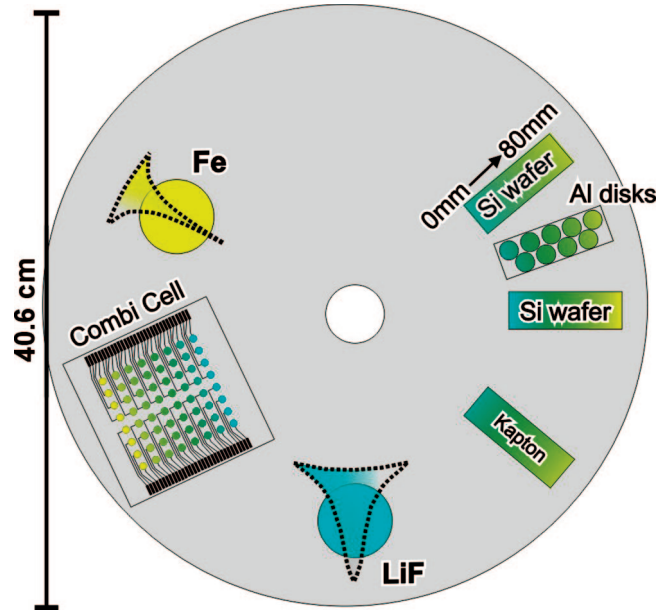

Figure 1. Layout of the combinatorial sputtering table. Substrates mounted include one combinatorial electrochemical cell, an array of Al foil disks for mass per unit area determination, two silicon substrates, and 13 Kapton substrates. Two targets are also indicated. The Fe target has a "linear out" mask, while the LiF target has a "linear in" mask.

are reported. The electrochemical activity of the library was studied using a 64-electrode electrochemical cell.[17,18] The structure and composition of the library were characterized by XRD, Mössbauer effect spectroscopy, and electron microprobe analysis.

Experiment

$[LiF]_{1-x}Fe_x$ nanocomposite libraries were made by magnetron cosputtering using a Corona Vacuum Coater's (Vancouver, BC, Canada) V3T system. The system holds up to five targets, is turbopumped, and has a typical base pressure for deposition around 1×10^{-7} Torr. 50 mm diameter targets of LiF and Fe were used. The sputtering chamber is equipped with a 40 cm diameter water-cooled rotating substrate table. Stationary masks are placed over individual targets to control the deposition profiles of the sputtered elements.[19] The chamber pressure was maintained at 1.0 mTorr of argon during the deposition. The substrate table angular speed was ~15 rpm.

As shown in Figure 1, the LiF and Fe sputtering targets were covered with masks designed to give a combinatorial thin-film library with the amount of LiF and the amount of Fe changing approximately linearly in opposite directions. As the substrate passes over the LiF and Fe targets, only about one monolayer of molecules or atoms is deposited so that the LiF molecules and Fe atoms are intimately mixed. Details of the sputtering procedure and modifications to the machine to enable combinatorial sputtering have been previously described.[19] For all films discussed in this paper, LiF was deposited using a radio-frequency (rf) power supply with a power of 160 W. The Fe was sputtered using a dc power supply at 30 W.

(5) Obrovac, M. N.; Dahn, J. R. *Electrochem. Solid-State Lett.* **2002**, *5*, A70.
(6) Amatucci, G. G. US Patent Application Publication US2004/0121235 A1, June 24, 2004.
(7) Zhou, Y. N.; Liu, W. Y.; Xue, M. Z.; Yu, L.; Wu, C. L.; Wu, X. J.; Fu, Z. W. *Electrochem. Solid-State Lett.* **2006**, *9*, A147.
(8) Zhou, Y. N.; Wu, C. L.; Zhang, H.; Wu, X. J.; Fu, Z. W. *Acta Phys.-Chim. Sin.* **2006**, *22*, 1111.
(9) Liao, P.; Mar, R.; Dahn, J. R. Abstract 339 presented at the 210th Electrochemical Society Meeting, Cancun, Mexico, Nov 2, 2006.
(10) Dunlap, R. A.; Deschamps, N. C.; Mar, R. E.; Farrell, S. P. *J. Phys.: Condens. Matter* **2006**, *18*, 4907.
(11) Todd, A. D. W.; Dunlap, R. A.; Dahn, J. R. *J. Alloys Compd.* **2007**, *443*, 114.
(12) Alcántara, R.; Jaraba, M.; Lavela, P.; Tirado, J. L.; Jumas, J. C.; Olivier-Fourcade, J. *Electrochem. Commun.* **2003**, *5*, 16.
(13) Bomio, M.; Lavela, P.; Tirado, J. L. *ChemPhysChem* **2007**, *8*, 1999.
(14) Kamali-M, S.; Ericsson, T.; Wäppling, R. *Thin Solid Films* **2006**, *515*, 721.
(15) Xiang, X. D.; Sun, X.; Briceno, G.; Lou, Y.; Wang, K. A.; Chang, H. Y.; Wallace-Freedman, W. G.; Chen, S. W.; Schultz, P. G. *Science* **1995**, *268*, 1738.
(16) Fleischauer, M. D.; Hatchard, T. D.; Bonakdarpour, A.; Dahn, J. R. *Meas. Sci. Technol.* **2005**, *16*, 212.
(17) Cumyn, V. K.; Fleischauer, M. D.; Hatchard, T. D.; Dahn, J. R. *Electrochem. Solid-State Lett.* **2003**, *6*, 15.
(18) Fleischauer, M. D.; Hatchard, T. D.; Rockwell, G. P.; Topple, J. M.; Trussler, S.; Jericho, S. K.; Jericho, M. H.; Dahn, J. R. *J. Electrochem. Soc.* **2003**, *150*, A1465.
(19) Dahn, J. R.; Trussler, S.; Hatchard, T. D.; Bonakdarpour, A.; Mueller-Neuhaus, J. R.; Hewitt, K. C.; Fleischauer, M. D. *Chem. Mater.* **2002**, *14*, 3519.

Continuous thin-film $[LiF]_{1-x}Fe_x$ libraries were deposited on two Si (100) wafers, a linear array of 1.3 cm diameter preweighed Al foil disks, one combinatorial cell plate, and 13 pieces of 25 μm thick Kapton film (each 25 mm × 100 mm) for the Mössbauer measurements.[19] One Si wafer was used for X-ray diffraction studies of the deposited material, and the other Si wafer was used to determine elemental composition versus position on the library using an electron microprobe. The Al foil disks were used to determine the mass per unit area deposited as a function of position on the library. Weights were measured before and after sputtering using a Cahn 29 microbalance. The data were fitted to obtain mass/unit area versus library position. The mass of material on each of the 64 electrode pads in the combinatorial cell was obtained on the basis of the position of the pad during sputtering, the pad area, and the function determined above. The combinatorial cell plate was used to characterize the electrochemical behavior of the samples.

One library deposited on a Si (100) wafer was used in XRD experiments to determine the structure as a function of position across the film. XRD measurements were performed using an INEL CPS120 curved position-sensitive detector coupled to an X-ray generator equipped with a Cu target X-ray tube. A monochromator in the incident beam path limits the wavelengths striking the sample to Cu Kα. The detector measures the entire diffraction pattern between scattering angles of 6° and 120° at once. The film sample is placed on an $x-y$ translation stage that allows measurement and movement operations to be sequentially programmed. Typically, XRD data were collected over the 76 mm long libraries with a spacing of 4 mm, leading to 19 patterns per library. Typical measurement times were 20 min per point on the library. The X-ray beam makes a spot about 1 mm (in the varying composition direction) by 3 mm (in the constant composition direction) in size on the library.

Films deposited on the other Si wafer substrate were used in electron microprobe experiments to determine composition as a function of position across the film. Electron microprobe measurements were made using a JEOL JXA-8200 superprobe. The microprobe is also equipped with a programmable $x-y$ stage which allows the composition to be measured on the same equally spaced points as those where the diffraction patterns were collected. Fe and F contents were measured with wavelength dispersive spectroscopy.

Room temperature ^{57}Fe Mössbauer effect spectra were collected using a Wissel System II spectrometer operating in the constant acceleration mode. A ^{57}Co source was used, and the velocity scale was calibrated relative to room temperature α-Fe. Thirteen layers of film deposited onto Kapton substrates were compositionally aligned and attached together to form the absorber. The absorber was then moved inside a helium-filled glovebox and sealed between aluminized polyester sheets with a heat sealer to prevent subsequent air exposure during the extended time needed to collect all the Mössbauer spectra. Nine spectra were obtained by moving the sample in front of a 4.5 mm × 25 mm lead aperture. Approximately a 6% range of the full composition spread was sampled at each step by using the 4.5 mm aperture. Data acquisition times at each position were typically 24–36 h. More details of the combinatorial Mössbauer technique are available in the literature.[10]

The combinatorial cell plate was used in the construction of a 64-electrode combinatorial electrochemical cell.[17,18] This consists of an aluminum base that holds the cell plate and a stainless steel cap, which was bolted on the base plate. The stainless steel cap contains a silicone O-ring to prevent leaks. The cell was assembled by first placing the cell plate on the aluminum base. Next, 1.0 mL of 1 M $LiClO_4$ (Aldrich) in 33:67 ethylene carbonate/diethyl carbonate (Ferro Corp.) (EC/DEC) electrolyte was added. A sheet of microporous polypropylene (Celgard 2502) was then laid on top of the cell plate to act as a separator. The separator was then covered by lithium foil to be used as a common counter and reference electrode. The stainless steel cap was then bolted down. This assembly procedure was completed in an argon-filled glovebox. The combinatorial electrochemical cell was then removed to air and cycled using a multichannel pseudopotentiostat described in ref 17.

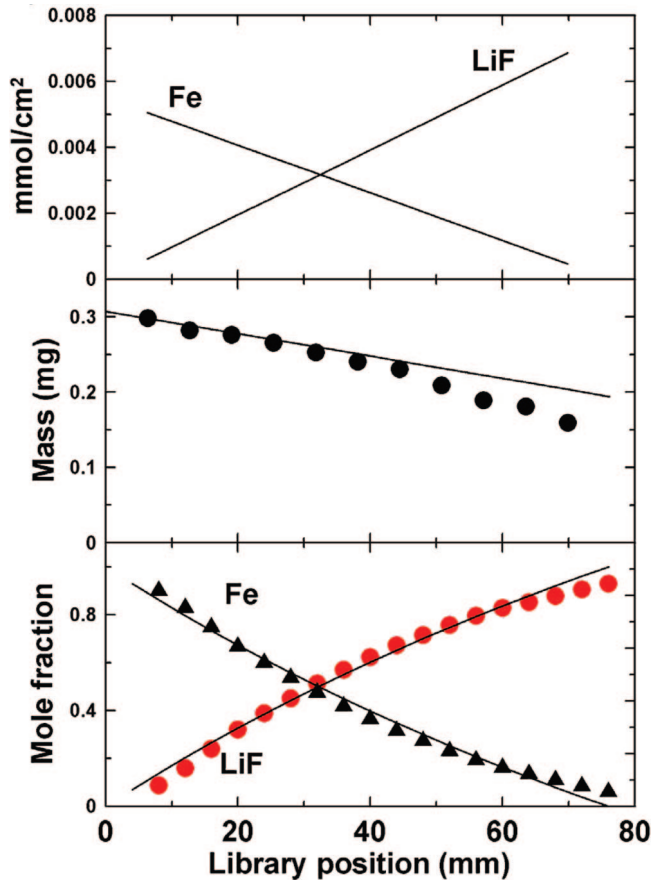

Figure 2. Theoretical and experimental compositions of the $[LiF]_{1-x}[Fe]_x$ ($0 < x < 1$) libraries. The top panel shows the calculated Fe and LiF moles per unit area defined by the "linear in" and "linear out" sputtering masks. The middle panel shows that the calculated mass per weighing disk (based on the top panel) agrees with the measured mass. The bottom panel shows that compositions calculated from the top panel agree with the measured compositions from wavelength dispersive spectroscopy.

The electrochemical cycling protocol for all cells tested was the same. After assembly, cells were held at open circuit (usually around 2.6 V) for 10 min and then charged from open circuit to 4.0 V with a sweep rate of 58 μV/s. After being held at 4.0 V for 10 min, the potential was swept linearly down to 1.2 V over 13 h 26 min (also 58 μV/s). Then the potential was held at 1.2 V for 10 min. The potential was then swept linearly from 1.2 to 4 V over 13 h 26 min. These results were integrated numerically to obtain the specific capacity versus potential for the first and second discharge cycles. Cells were tested at 70 °C in a small muffle oven.

Results and Discussion

Two methods were used to obtain the composition of the $[LiF]_{1-x}[Fe]_x$ ($0 < x < 1$) library. Figure 2 shows the theoretical and measured compositions of the $[LiF]_{1-x}[Fe]_x$ library plotted as a function of position along the library. The theoretical compositions were calculated from the linear

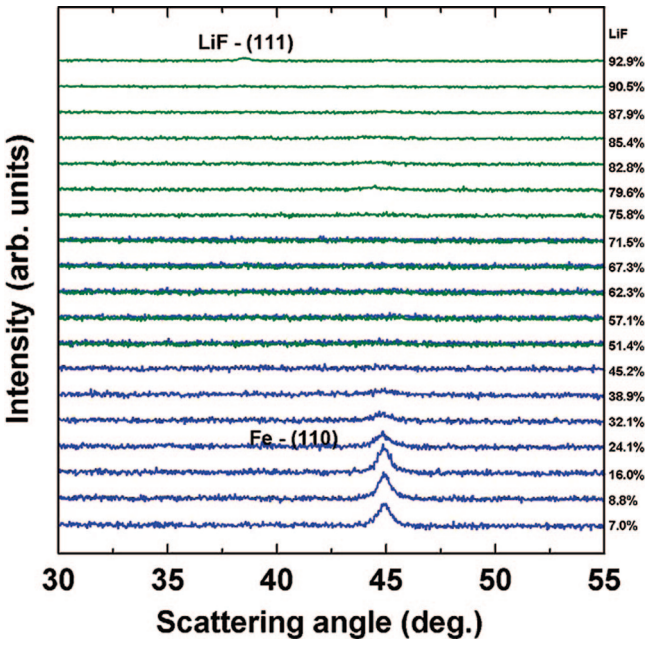

Figure 3. XRD patterns collected from 19 different positions in the $[LiF]_{1-x}[Fe]_x$ ($0 < x < 1$) libraries. The left y-axis is the X-ray intensity, and the right y-axis indicates an estimate of the mole percent of LiF corresponding to each pattern.

variations of the LiF and Fe mass per unit areas defined by the linear in and linear out sputtering masks as

$$\text{mass/area} = \left[A\left(\frac{y}{76}\right)(6.94 + 19.00) + B\left(\frac{76 - y}{76}\right) \times 55.85\right] \quad (1)$$

The constants A and B are the maximum number of mol/cm^2 of LiF deposited (at $y = 76$ mm) and the maximum number of mol/cm^2 of Fe deposited (at $y = 0$ mm), respectively. The constants 55.85, 6.94, and 19.00 g/mol are the molar masses of Fe, Li, and F. The parameter, y (in mm), measures the position along the library with $y = 0$ at the Fe end of the 76 mm long library. The top panel of Figure 2 shows the calculated mol/cm^2 of LiF and Fe plotted as position along the library. The middle panel shows that the calculated mass and measured mass of the sputtered film on the 1.3 cm diameter disks agree well. The bottom panel shows that the composition derived from the mol/cm^2 in the top panel is in good agreement with the composition measured by wavelength dispersive spectroscopy (WDS). This gives us confidence that we understand the composition versus position of the library.

Figure 3 shows 19 XRD patterns collected at different positions along the $[LiF]_{1-x}[Fe]_x$ ($0 < x < 1$) library on the silicon substrate. The graph shows the X-ray intensity on the left y-axis and an estimate of LiF mole percent for each pattern determined from the electron microprobe results on the right y-axis. The thickness of the library ranges between ~500 nm at the LiF end to ~300 nm at the Fe end, as determined using a Dektak 8 profilometer. For the XRD pattern collected from material containing 92.9% LiF ($[LiF]_{0.93}[Fe]_{0.07}$), the peak at 38.5° is attributed to the LiF (111) Bragg peak. For the material containing 7% LiF (93% Fe), the diffraction peak at 44.7 was assigned to Fe (110). The XRD patterns collected from material with LiF percentage ranging from 45.2% to 75.8% do not show any Fe or LiF peaks. From 79.6% to 90.5% LiF, the material shows a very broad peak at 44.9° thought to arise from LiF (200). The materials in the middle of the library are therefore highly nanostructured or amorphous.

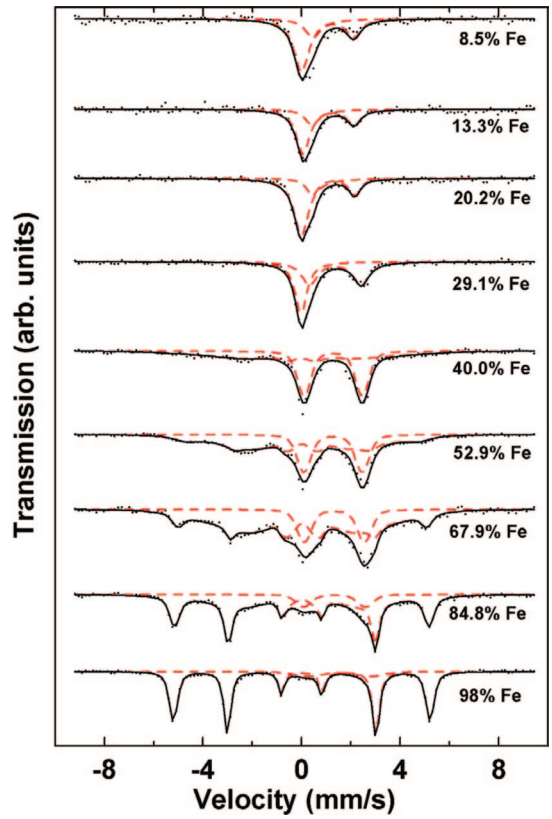

Figure 4. Room temperature ^{57}Fe Mössbauer spectra of the $[LiF]_{1-x}[Fe]_x$ ($0 < x < 1$) library as a function of Fe content. The velocity scale is measured relative to room temperature α-Fe. Fe percent is shown below each spectrum. Solid lines through the data represent the total fits, and the dashed lines are the spectral components.

Figure 4 shows the Mössbauer spectra of the $[LiF]_{1-x}[Fe]_x$ ($0 < x < 1$) library as a function of Fe content. For 98 to 40 at. % Fe, the Mössbauer spectra were fit to a sextet and a doublet with Voigt-based functions (VBF).[20] When the Fe content falls between 29.1 and 8.5 mol %, the Mössbauer spectra were fit to a Lorentzian singlet and a Lorentzian doublet. The parameters of these components are listed in Table 1. A model is illustrated in Figure 5 to explain the Mössbauer effect spectra. At the Fe-rich end of the library, small LiF regions are surrounded by large Fe grains with some interfacial regions between them. The VBF sextet is symmetric and has zero center shift, which means it originates most probably from Fe atoms located inside the large Fe grains which are surrounded by neighboring Fe atoms. The Fe neighbors generate an internal magnetic field at the nuclei of the central Fe atoms and cause the sextet splitting. Within the interfacial regions, Fe atoms have asymmetric environments composed of Fe, F, and Li atoms. These asymmetric environments create electric field gradients at the Fe nuclei, which produce quadrupole splitting. Table

(20) Dunlap, R. A.; Lawther, D. W.; Hargraves, P.; Sinclair, P. *J. Phys. F: Met. Phys.* **1988**, *18*, 2479.

Table 1. Center Shifts, Internal Magnetic Field, Quadrupole Splitting, and Site Populations for the Sextet, Doublet, and Singlet Subspectra Used To Fit the Mossbauer Spectra of the $[LiF]_{1-x}Fe_x$ Library Members[a]

	sextet			doublet			singlet		
Fe atomic percent (%)	center shift (mm/s)	H (T)	fraction (%)	center shift (mm/s)	quadrupole splitting (mm/s)	fraction (%)	center shift (mm/s)	fraction (%)	goodness of fit (χ^2)
98.0	0.0	32.3	90.3	1.50	2.49	9.7			2.46
84.8	0.0	27.9	88.7	1.34	2.50	11.3			1.48
67.9	0.0	22.1	79.3	1.33	2.44	20.7			1.60
52.9	0.0	20.8	66.3	1.28	2.36	33.7			26.15
40.0	0.0	20.6	48.8	1.28	2.35	51.2			2.54
29.1				1.37	2.10	53.6	0.0	46.4	1.20
20.2				1.29	1.72	31.1	0.0	68.9	1.04
13.3				1.28	1.70	40.6	0.1	59.4	0.89
8.5				1.27	1.66	39.8	0.0	60.2	9.22

[a] The goodness of fit between the calculated spectrum and the data is also given.

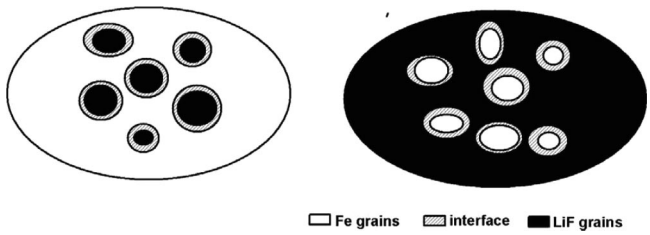

Figure 5. Schematic illustration of the nanostructures of the Fe-rich end (left) and the LiF-rich end (right) of the $[LiF]_{1-x}[Fe]_x$ ($0 < x < 1$) libraries. Fe grains are shown in white, LiF grains are shown in black, and the interfaces are shown in the hatched regions.

1 shows that when the LiF content increases, the quadrupole splitting of the doublet decreases from 2.49 to 1.66 mm/s and the center shift decreases from 1.50 to 1.27 mm/s. The center shift of the interfacial doublet is close to that found in FeF_2, which has the rutile structure with the iron coordinated by six fluorine atoms (quadrupole splitting = 2.79 mm/s, center shift = 1.37 mm/s).[21] This large positive center shift of the doublet indicates that Fe atoms within interfacial region have been oxidized by neighboring F atoms. However, the different quadrupole splitting between the interfacial Fe atoms and FeF_2 suggests that the interfacial Fe atoms have different environment from those Fe atoms in FeF_2. Since the interfacial Fe atoms must donate some electrons to neighboring F atoms, the Li:F ratio within interface region must be less than 1. Because there is thought to be no lithium loss during sputtering, the extra Li atoms must be stored on the LiF side of the interface.[22] It is worth noting that none of the fitted components matched Fe oxides, suggesting that the amount of Fe oxide in the $[LiF]_{1-x}[Fe]_x$ library was negligible.

At the LiF-rich end of the library, the existence of large LiF grains prevent small Fe grains from aggregating. Because the Fe grains are so small, the Fe atoms within these grains are superparamagnetic, not ferromagnetic. In this case, the central portion of the Fe nanograins now show a singlet in the Mössbauer spectra while the Fe atoms within the interfacial region still show a doublet. According to ref 23, the upper limit of superparamagnetic Fe grain size at a particular temperature, T_b, called the blocking temperature, can be calculated using the following equation:

$$V = \frac{K_B T_b}{2K} \ln\left[\frac{2KA\tau_L}{\rho N_0 h}\right] \quad (2)$$

where V is the grain volume, K is the magnetocrystalline anisotropy constant, A is the atomic weight, ρ is the density, N_0 is Avogadro's number, h is Planck's constant, k_B is Boltzmann's constant, and τ_L is the Mössbauer effect intermediate-state lifetime. The excited-state properties of a ^{57}Fe nucleus gives $\tau_L \approx 3.2 \times 10^{-8}$ s. A specific value for the magnetocrystalline anisotropy is not available for superparamagnetic Fe. However, for estimation purposes, $K = 5.0 \times 10^4$ J m^{-3}, obtained by extrapolating K for aluminum iron alloys to zero aluminum content, was used.[24] For Fe, $A = 55.85 \times 10^{-3}$ kg/mol and ρ is 7874 kg m^{-3}. According to ref 23, $T_b = 270$ K if the site populations of ferromagnetic and superparamagnetic components are equal at 270 K. Figure 4 shows that the material with 40 at. % Fe has a ferromagnetic sextet and an interfacial doublet, while the material with 29.1 at. % Fe has a superparamagnetic singlet and an interfacial doublet. Therefore, some composition between 29.1 and 40 at. % Fe must have $T_b = 270$ K. Thus, using eq 2, the upper limit of superparamagnetic Fe grain size is around 6.6 nm at 270 K, meaning the Fe grains must be less than 6.6 nm in order to be superparamagnetic at 270 K. In the middle of the library, where LiF and Fe atoms are intimately mixed, Fe atoms are about equally distributed within the Fe grains and the interfacial region.

The estimate of grain size for compositions near 35% Fe described above can be compared to the Fe grain size measured using X-ray diffraction. Figure 3 shows that the full width of the broad Fe (110) peak is $1.6 \pm 0.3°$ (obtained by least-squares fitting of a Lorentzian line shape) for the material containing 38.9% LiF (61.1% Fe). The instrumental resolution is 0.13° as determined by measurements on a crystalline corundum standard. The instrumental resolution was subtracted from the measured peak widths and then the result was used to calculate the grain size. Using the Scherrer equation

$$L = \frac{0.9\lambda}{B_{(2\theta)} \cos\theta} \quad (3)$$

(where λ is the Cu Kα wavelength (0.154 nm), $B_{(2\theta)}$ is the full width at half-maximum of the Bragg peak, and θ is the

(21) Wertheim, G. K. *Phys. Rev.* **1961**, *121*, 63.
(22) Liao, P.; Dunlap, R. A.; Dahn, J. R., submitted to *J. Phys.: Condens. Matter*.
(23) Dunlap, R. A.; Alghamdi, A.; O'Brien, J. W.; Penney, S. J. *J. Alloys Compd.* **2004**, *365*, 84.
(24) Hall, R. C. *J. Appl. Phys.* **1959**, *30*, 816.

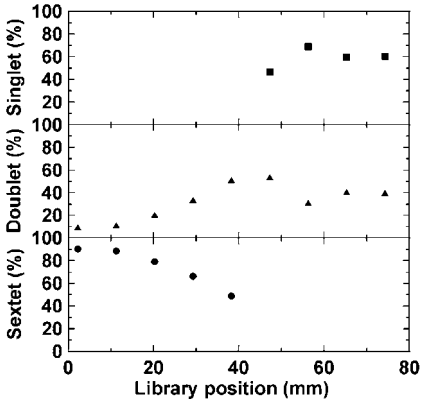

Figure 6. Site populations of different components as a function of library position as measured by room temperature ^{57}Fe Mössbauer spectroscopy.

Bragg angle), the average Fe grain size at a composition of $[LiF]_{0.389}Fe_{0.611}$ is estimated to be 6 ± 1 nm. This is close to the estimate of 6.6 nm from Mössbauer spectroscopy for the composition (between 29.1 and 40 at. % Fe) with a blocking temperature near 270 K. Figure 3 shows that as the LiF content increases, the size of the Fe grains decreases below 6 nm because the Fe (110) Bragg peak becomes even broader and more difficult to observe.

Figure 6 shows the site populations of the sextet, doublet, and singlet. When the Fe content is reduced from 98 to 40 mol %, the sextet population decreases from 90.3 to 48.8% while the doublet population increases from 9.7 to 51.2%. After the Fe percentage falls below 40 mol %, the sextet disappears, and a singlet appears in the middle of the Mössbauer spectra, whose population remains about constant while the Fe content reduces from 29.1 to 8.5 mol %.

The changes in Figure 6 can be explained on the basis of the model shown in Figure 5. The Fe grain sizes become smaller when the mole percent of LiF increases. Supposing the width of interfacial region is constant, then the percentage of central Fe atoms, which correspond to the sextet, must decrease and then become zero when Fe grains reduce in size to the superparamagnetic range. Within the superparamagnetic region, the ratio between singlet population and doublet population remains constant because apparently the size of the Fe grains does not change too much over this range.

Figure 7 shows the distribution of the internal magnetic field of the sextet component in the Mössbauer spectra. Below each distribution there is a thin dashed horizontal line which shows the zero of the probability distribution. When the Fe content is around 98 mol %, the internal magnetic field has a sharp peak around 32.32 T, indicating large Fe grains. As the Fe content decreases, the distribution broadens gradually and the intensities become smaller, indicating continually decreasing Fe grain sizes.

Figure 8 shows the differential capacity versus potential (dQ/dV vs V) of a 64-electrode combinatorial electrochemical cell heated to 70 °C. The channels in the top row of the 64-electrode cell (channels 1, 9, 17, 25, 33, 41, 49, and 57) exhibit virtually no capacity. This is consistent with the fact that these eight channels are at the Fe-rich end of the library, and the positive electrode

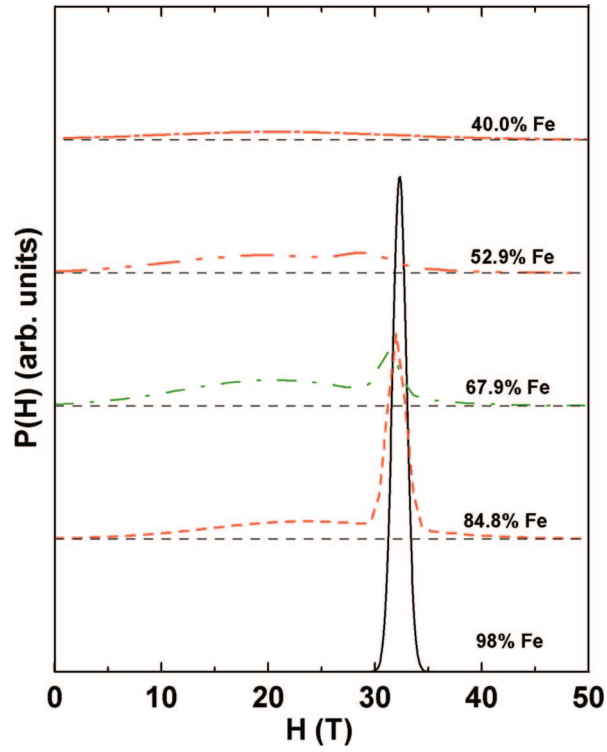

Figure 7. Measured room temperature ^{57}Fe Mössbauer internal magnetic field distributions, $P(H)$, as a function of Fe content. The thin dashed horizontal line below each distribution shows the zero of the probability distribution. Fe mole percent is indicated near each distribution.

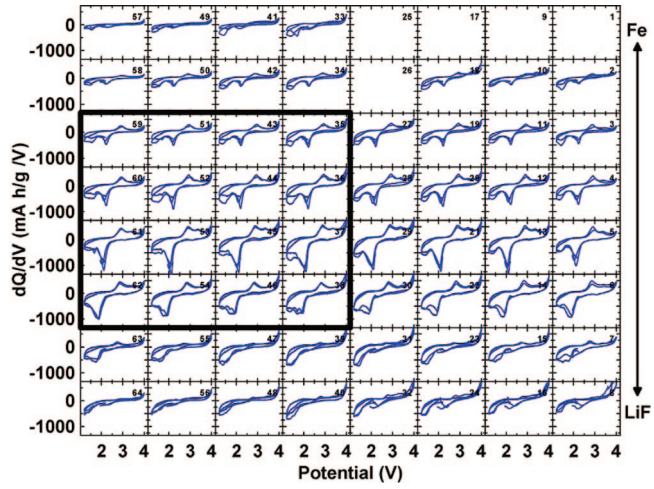

Figure 8. Differential capacity versus potential between 1.2 and 4 V for the first several charge–discharge cycles of a 64-electrode combinatorial cell. Slow linear sweep voltammetry (58 μV/s) was used. Each charge or discharge took 13 h 26 min using this sweep rate. The Fe content in the $[LiF]_{1-x}[Fe]_x$ ($0 < x < 1$) library increases toward the top of the figure, and the LiF content increases toward the bottom. The top row is almost pure Fe, and the bottom row is almost pure LiF. The electrode number is indicated in each panel.

material in these channels is basically pure Fe. Pure Fe has no capacity between 1.2 and 4 V. Similarly, the bottom row of the 64 channels (channels 8, 16, 24, 32, 40, 48, 56, and 64) also shows little electrochemical activity because the positive electrode material on these channels is basically pure LiF. However, in the middle of the 64-electrode combinatorial cell, where the positive electrode materials are $[LiF]_{1-x}Fe_x$ nanocomposites, very good electrochemical activities are observed.

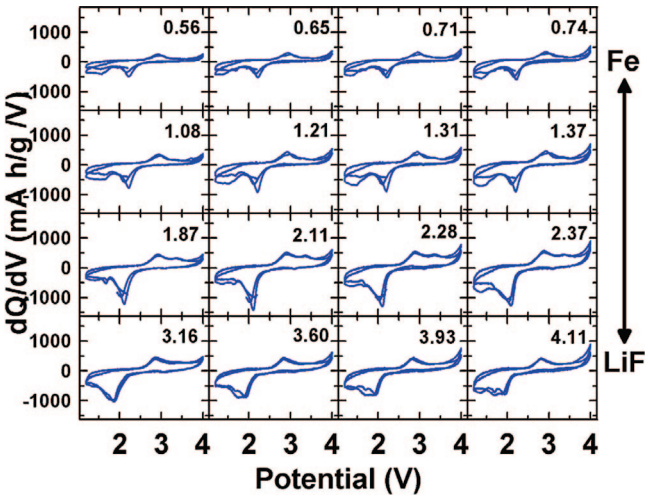

Figure 9. Differential capacity versus potential between 1.2 and 4 V for the 16 highlighted electrodes in Figure 8. The LiF:Fe atomic ratio is given at the upper right of each panel.

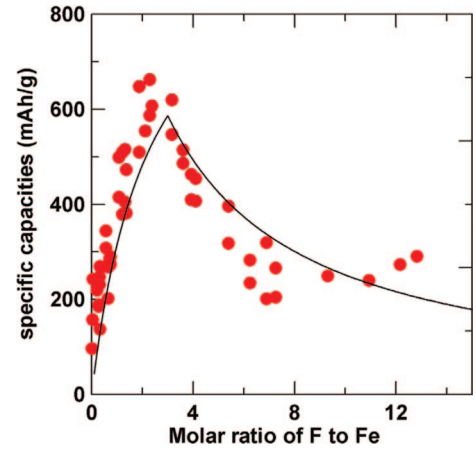

Figure 10. Theoretical and experimental second discharge capacity of the $[LiF]_{1-x}[Fe]_x$ ($0 < x < 1$) libraries versus the lithium fluoride-to-iron ratio. The solid curve is the prediction based on the formation of FeF_3 at the top of charge. The circles show the experimental results from the cell described by Figures 8 and 9.

Figure 9 is an expanded view of the data for the 16 electrodes outlined by the heavy black box in Figure 8. The F to Fe ratio is indicated in each panel of Figure 8. All 16 electrodes show oxidation peaks around 2.94 V, while the main reduction peaks for the 16 channels range from 2.22 to 1.95 V. There may be many reasons for the shift of the reduction peaks. One possible reason is that at the Fe-rich end of the library the material contains more Fe nanometal. Fe nanometal has good electrical conductivity and thus may help to reduce the charge–discharge hysteresis of the nanocomposite. Another possible explanation for the reduction in hysteresis is that different ranges of the library may have different final products. FeF_2 and FeF_3 may coexist within the Fe-rich end of the library while at the LiF-rich end only FeF_3 may exist. We are planning to do in situ Mössbauer experiments on Li/$[LiF]_{1-x}Fe_x$ cells to discern the final products. In addition to the main pair of oxidation and reduction peaks, all 16 channels show some discharge capacity below 1.8 V, which appear as humps below 1.8 V in Figure 9. This extra reversible capacity may come from Li storage in the newly formed LiF/Fe boundaries.[25,26] Similar results have been found when discharging Li/RuO_2 cells.[27,28] Another possible reason for this extra reversible capacity could be reversible formation of an SEI layer as was proposed for the extra capacity in Li/CoO cells.[29] However, the lower cutoff voltage of our 64-channel combi cell was 1.2 V, so we seriously doubt that a reversible SEI film can form at such high voltage.

On the basis of the displacement reaction nLiF + Fe ↔ FeF_n + nLi, a simple model was proposed to calculate the specific capacities of the $[LiF]_{1-x}Fe_x$ nanocomposites. Assuming FeF_3 ($n = 3$) is the final product, then if the LiF to Fe ratio is larger than 3 ($x < 0.25$), all the Fe will be converted into FeF_3, leaving excess LiF, and the specific capacity, Q, of the $[LiF]_{1-x}Fe_x$ nanocomposite will be

$$Q = \frac{3 \times 26700\ (\text{mA h/mol})}{55.85 + (6.94 + 19.00)\frac{1-x}{x}\ (\text{g/mol})} \quad (4)$$

If the LiF to Fe ratio is less than 3 ($x > 0.25$), then all the F will react with Fe when the Li is removed, leaving excess Fe, and the specific capacity of the $[LiF]_{1-x}Fe_x$ nanocomposite will be

$$Q = \frac{\frac{1-x}{x} \times 26700\ (\text{mA h/mol})}{55.85 + (6.94 + 19.00)\frac{1-x}{x}\ (\text{g/mol})} \quad (5)$$

In eqs 4 and 5, 55.85, 6.94, and 19.00 g/mol are the molar masses of Fe, Li, and F, respectively, and 26 700 mA h/mol is Faraday's number.

Figure 10 shows the theoretical and experimental second discharge capacities of the $[LiF]_{1-x}Fe_x$ library plotted versus the LiF:Fe ratio, $(1 - x)/x$. The solid curve shows the theoretical capacity if the product after lithium extraction is FeF_3, which has a maximum value at F:Fe = 3. The experimental capacities also show a peak around F:Fe = 3, which strongly suggests that the final product is FeF_3. When the F:Fe ratio is less than or equal to 3, the experimental capacities are higher than the theoretical values. The extra capacity may come from Li storage in the newly formed LiF/Fe boundaries.[25–28]

Conclusions

In this work, highly electrochemically active thin film $[LiF]_{1-x}[Fe]_x$ ($0 < x < 1$) nanocomposite libraries were prepared by combinatorial magnetron sputtering. XRD shows that Fe grains are within nanometer ranges and that their size decreases as the LiF mole percentage increases. In the middle of the library where the material shows the best electrochemical activities, X-ray diffraction does not show any Fe or LiF peaks, while Mössbauer spectra show that Fe

(25) Maier, J. *Nat. Mater.* **2005**, *4*, 805.
(26) Li, H.; Richter, G.; Maier, J. *Adv. Mater.* **2003**, *15*, 736.
(27) Balaya, P.; Li, H.; Kienle, L.; Maier, J. *Adv. Funct. Mater.* **2003**, *13*, 621.
(28) Zhukovskii, Y. F.; Balaya, P.; Kotomin, E. A.; Maier, J. *Phys. Rev. Lett.* **2006**, *96*, 058302.
(29) Dedryvère, R.; Laruelle, S.; Grugeon, S.; Poizot, P.; Gonbeau, D.; Tarascon, J. M. *Chem. Mater.* **2004**, *16*, 1056.

atoms are about equally distributed within Fe grains and in the interfacial regions. At the LiF-rich end, Mössbauer spectra show that the Fe grain sizes fall into the paramagnetic region (less than 6.6 nm according to ref 23) because large LiF grains prevent the aggregation of small Fe grains. When the LiF:Fe ratio is 3.16, the material shows a second discharge specific capacity of 620 mA h/g at 70 °C. The measured second discharge capacities versus composition are in good agreement with the theoretical capacities if it is assumed that the final product is FeF_3. The extra capacity in materials with high Fe content may arise from Li stored in the newly formed LiF/Fe boundaries according to the ideas presented in refs 25−28.

Some phenomena regarding the potential vs specific capacity relations of $Li/LiClO_4/[LiF]_{1-x}Fe_x$ cells are still not fully understood. Most important is to understand the reason for the large charge–discharge hysteresis observed in these materials. Steps can then be taken to reduce the hysteresis. $[LiF]_{1-x}Fe_x$ nanocomposites are nanostructured or amorphous materials, and therefore Li ion transport is presumably quite different from that which takes place in intercalation compounds like $LiCoO_2$ and $LiFePO_4$. Some basic transport experiments on $[LiF]_{1-x}Fe_x$ nanocomposites are recommended as future work. Nanocrystalline metals within electrochemical cells can grow in size due to the "electrochemical Ostwald ripening" effect.[30] This will cause capacity fading in $Li/[LiF]_{1-x}Fe_x$ cells since Fe atoms within the core of large particles will not take part in the displacement reaction. Using in situ Mössbauer effect spectroscopy experiments at the end of each discharge cycle, the ratio between the number of core Fe atoms and interfacial Fe atoms can be determined. If this ratio increases with cycle number, such experiments will support the "electrochemical Ostwald ripening" effect.

Acknowledgment. The authors acknowledge the support of this research by NSERC and 3M Canada under the auspices of the Industrial Research Chair program.

CM702656K

(30) Schröder, A.; Fleig, J.; Gryaznov, D.; Maier, J.; Sitte, W. *J. Phys. Chem. B* **2006**, *110*, 12274.